

1
2
3
4
5
6
7
8
9
10
11
12
13
14
15
16
17
18
19
20
21

Controls on the development and termination of failed continental rifts: Insights from the crustal structure and rifting style of the North Sea via ambient noise tomography

E. Crowder^{1,*}, N. Rawlinson², D. G. Cornwell¹, C. Sammarco¹, E. Galetti⁴, A. Curtis^{3,4}

This manuscript is a **preprint** and has been submitted for publication in **Earth and Planetary Science Letters (EPSL)**. Please note that, not having undergone peer-review, the manuscript has yet to be formally accepted for publication. Subsequent versions of this manuscript may have slightly different content. If accepted, the final version of this manuscript will be available via the *'Peer-reviewed Publication DOI'* link on the right-hand side of this webpage. Please feel free to contact any of the authors; we welcome feedback

22 **Controls on the development and termination of failed continental rifts:**
23 **Insights from the crustal structure and rifting style of the North Sea via**
24 **ambient noise tomography**

25

26 E. Crowder^{1,*}, N. Rawlinson², D. G. Cornwell¹, C. Sammarco¹, E. Galetti³, A. Curtis^{3,4}

27

28

29 1. School of Geosciences, University of Aberdeen, Aberdeen AB24 3UE, Scotland,

30 United Kingdom

31 2. Department of Earth Sciences, University of Cambridge, Cambridge, CB3 0EZ,

32 United Kingdom

33 3. School of Geosciences, University of Edinburgh, Edinburgh, EH8 9XP, United

34 Kingdom

35 4. Institute of Geophysics, ETH Zurich, Zurich, Switzerland

36

37* Corresponding author. Email address: emily.crowder@abdn.ac.uk (E. Crowder)

38

39

40**Abstract**

41 The mid to lower crust plays an important role in rift initiation and evolution,
42 particularly when large scale sutures and/or terrane boundaries are present. These inherited
43 features can focus strain or act as inhibitors to extensional deformation. Ancient tectonic
44 features are known to exist beneath the iconic failed rift system of the North Sea making it
45 the ideal location to investigate the complex interplay between pre-existing regional
46 heterogeneity and rifting. To this end, we produce a 3D shear-wave velocity model from
47 transdimensional ambient seismic noise tomography to constrain crustal properties to ~30 km
48 depth beneath the North Sea and its surrounding landmasses. Major North Sea sedimentary
49 basins appear as low shear-wave velocity zones that are a good match to published sediment
50 thickness maps. We constrain relatively thin crust (13-18 km) beneath the Central Graben
51 depocentres that contrasts with crust elsewhere that is at least 25-30 km thick. Significant
52 variations in rift style and structure are identified along the failed rift system, varying
53 between symmetric and strongly asymmetric extension, that is related to the location of
54 Laurentia-Avalonia-Baltica paleo-plate boundaries. We identify clear variations between

55paleo-plates with strong lateral gradients in crustal velocity related to Laurentia-Avalonia-
56Baltica plate juxtaposition and reduced lower crustal velocities in the vicinity of the Thor
57suture, possibly representing the remnants of a Caledonian accretionary complex. Our results
58provide fresh insight into the pivotal role that ancient terranes can play in the formation and
59failure of continental rifts, and may help explain the failure of other similar continental rifts
60such as Bass Strait in Australia.

61

62**Key words**

63Seismic tomography

64Seismic noise

65Bayesian inversion

66North Sea

67Crustal structure

68Rifting

69

70**1. Introduction**

71 Continental areas subject to extensional stresses may eventually rift as the lithosphere
72becomes stretched and thinned. After undergoing extension for a prolonged period, a
73continental rift can ultimately achieve full breakup and transition to seafloor spreading.
74However, this stage is often never reached and a new mid-ocean rift does not form. The
75reasons why some rifts fail and others succeed are unclear; however, the mechanical strength
76and presence of pre-existing heterogeneity, including old sutures and faults, may be of
77primary importance. Understanding failed rift systems is important for understanding how
78plate tectonics operate on Earth more generally, but there is also an economic consideration
79in the form of the vast reserves of oil and gas that they host (e.g. Bass Strait, Australia; Benue
80Trough, Nigeria and the North Sea). While the structure of the uppermost crust and its
81extensional faulting, basin formation and hydrocarbon reservoirs tends to be well mapped and
82understood in these areas, below the economic basement the deeper crust remains poorly
83constrained. This is particularly true of the North Sea, where only a handful of vintage, deep
84seismic reflection/refraction profiles of varying quality have been collected and interpreted
85(e.g. Pharaoh, 1999). Yet, if we are to understand how rifts form and why they fail, it is
86crucial to have a first-order knowledge of rift geometry, large-scale pre-rift architecture of the
87mid-lower crust and their interaction in order to assess the influence of pre-existing structures
88on rift initiation and evolution.

89 Prior to the formation of the North Sea, the northwest European Atlantic margin
90 recorded a long and complex tectonic history. As summarised by Ziegler (1990), numerous
91 extensional and orogenic events influenced the region since its initial formation during the
92 triple plate collision of palaeo-continentals in the Ordovician-early Devonian aged Caledonian
93 Orogeny. This occurred when the Thor Ocean between Avalonia and Baltica closed by
94 southward subduction under the north Avalonian margin (Torsvik and Rehnström, 2003).
95 Subsequently, oceanic subduction switched northward beneath the Laurentian margin as
96 Baltica-Avalonia moved towards Laurentia, closing the Iapetus Ocean in the late Silurian-
97 early Devonian. Later in the Devonian, a distal foreland basin formed in the central and
98 southern North Sea in response to the Variscan orogeny, which was focussed at the southern
99 margin of Avalonia. Carboniferous extension following the orogenies resulted in crustal
100 thinning, subsidence and successive sediment accumulation. From the Triassic to the Jurassic,
101 most of Europe was subject to the main rifting stage of the North Sea and several kilometres
102 of sediment accumulated in some basins. During the Cretaceous, rifting slowed and came to
103 an end, creating the North Sea failed rift system as the dominant regional stresses shifted
104 westward towards North America and the Proto-Atlantic opening. The location and
105 continuity of ancient collisional sutures and spatial extent of old/deep extensional zones are
106 uncertain and remain open to debate (e.g. Smit et al., 2016). Moreover, the failed rifting
107 events in the North Sea overprint and therefore complicate interpretation of these older, but
108 important crustal features.

109 To develop a better understanding of North Sea crustal structure and the potential
110 interplay of ancient sutures and continental rifting, we use ambient noise tomography to
111 create the first 3D shear-wave velocity model of the crust beneath the North Sea region. Prior
112 to this work, the North Sea has been included in large-scale regional tomographic studies of
113 Europe (e.g. Yang et al., 2007), where the horizontal resolution varies from ~100 km in the
114 southernmost North Sea to >800 km in the central North Sea and is therefore only
115 characterised by one or two broad scale velocity anomalies. In this study, we present a more
116 detailed model of the crust to ~30 km depth in which numerous well-constrained features are
117 recovered. We interpret the new model in the context of the crustal structure and tectonic
118 evolution of the region, with a particular focus on the influence of structural inheritance in the
119 development and cessation of rifting. We also compare our results with other rift systems
120 from around the world in an effort to draw broader conclusions on the role of pre-existing
121 heterogeneity in the origin and development of failed rift systems.

122

1232. Data and methods

124 Prior to this study, surface wave velocities were found to be virtually impossible to
125 extract from North Sea ambient noise data using conventional cross-correlation methods due
126 to the high noise levels and complexities of the recovered signal (Galetti et al., 2016;
127 Nicolson et al., 2014). However, by using recently developed processing techniques, we
128 successfully obtain group velocity dispersion measurements, which are then used in a robust
129 Bayesian, hierarchical, transdimensional tomography scheme to produce a new high-
130 resolution model of the 3D shear-wave velocity structure beneath the North Sea.

131 Data for this study come from 54 permanent seismic stations located in countries
132 surrounding the North Sea (Fig. 1). Both between and within the countries' networks there is
133 high variability in terms of sample rate, type of instrument and corner frequency (which can
134 limit the period range used in dispersion analysis). A major challenge for this dataset is the
135 highly attenuative nature of the crust below the North Sea, which has previously been
136 observed to dramatically reduce the signal-to-noise ratio of short (1-10 s) period surface
137 waves (Ventosa et al., 2017). In the 1-2 s period range, it has been suggested that extremely
138 high attenuation in the North Sea upper crust almost completely suppresses signal in ambient
139 noise cross-correlations (Allmark et al., 2018). In this study, we have a minimum period of 4
140 s, thereby avoiding the attenuation problem at the shortest periods. However, additional
141 challenges arise from the dominant source of noise possibly being within rather than outside
142 the study area (i.e. the Atlantic Ocean was assumed to be the main source, but the North Sea
143 itself may be a significant contributor of microseismic noise – see Nicolson et al., 2014). In
144 order to obtain high quality surface wave dispersion information, we use approximately five
145 years of continuous data recorded between 2010 and 2015 and apply a new phase-weighted
146 stacking technique (Schimmel et al., 2011), prior to carrying out ambient seismic noise
147 tomography of the North Sea.

148

1492.1. Preprocessing

150 The ambient noise cross-correlation procedure we employ is similar to that of Bensen
151 et al. (2007), and utilises MSNoise (Lecocq et al., 2014) for data preprocessing. Continuous
152 seismic recordings are split into hour long segments and carefully quality controlled by
153 removing files containing glitches (e.g. data gaps or unexplained spikes) and/or data streams
154 which are less than one-hour duration. To produce the highest-quality Green's functions, we
155 first remove the mean, the trend and the instrument response from the noise recordings of
156 vertical component traces. Subsequently, the mean and trend are removed again and a taper is

157applied to each trace. The final corrected traces are merged to form files containing 24 hours
158of data (or at least 90% of one full day). All daily traces are down-sampled to a uniform 1 sps
159in order to perform daily cross-correlations.

160

1612.2. Stacking

162 The daily cross-correlations and stacking processes are challenging aspects of this
163analysis largely due to the fact that the stations surround the North Sea, which itself is a
164major source of noise. This creates many artefacts in the cross-correlations that need to be
165excluded from further analysis. Tests on North Sea data show that phase cross-correlation
166(Schimmel et al., 2011) is the best approach for de-noising seemingly incoherent signals
167(Supplementary Fig. 1). To stack all the daily cross-correlations from the entire recording
168period for each station pair, time-domain phase weighted stacking (ts-PWS, Ventosa et al.,
1692017) was used (Supplementary Fig. 2). Phase-weighted stacking is a method based on
170analytic signal theory using the instantaneous phase at each given time on the signal envelope
171to optimally align traces (this is the phase that should be the same for coherent signals at each
172given time). When tested against the time-frequency domain PWS (Schimmel et al., 2011),
173results were very similar, but the ts-PWS was selected as the preferred method based on its
174significantly higher computational efficiency. A total of 1,275 empirical Green's functions
175were successfully extracted from the 54-station network (Supplementary Fig. 3).

176

1772.3. Dispersion analysis

178 We performed group velocity dispersion measurements using a multiple filtering
179technique (via Computer Programs in Seismology software; Herrmann, 2013) applied to the
180symmetric component (stack of the causal and acausal signals) of the negative time derivative
181of the cross-correlation functions, which can be interpreted as Rayleigh wave Green's
182functions. Group velocities were picked within a period range of 4 – 40 s (Fig. 2), and quality
183control is implemented via manual inspection of the 1,275 dispersion curves, which were
184categorised as "good", "fair" and "poor". The "poor" curves were deemed too noisy to pick.
185The "fair" curves were noisy but dispersion maxima could be picked with low confidence.
186The "good" curves had the clearest group velocity dispersion maxima and could be
187confidently picked. Out of 760 picked dispersion curves, all 614 of the "good" curves are
188used in the subsequent inversion (Fig. 2). To investigate the feasibility of obtaining phase
189velocities we applied automated frequency-time analysis using the image transformation
190technique described in Young et al. (2011). However, the resultant phase dispersion plots

191 were much noisier and less coherent than the equivalent group dispersion plots, which made
192 reliable picking extremely challenging (see Supplementary Fig. 4).

193

194 **2.4. Two-stage inversion**

195 After making the group velocity measurements, a series of tomographic inversions
196 were performed for even numbered periods between 4 and 40 s using the transdimensional,
197 hierarchical Bayesian inversion technique described by Young et al. (2013). For each period
198 of interest, the 2D group velocity model is dynamically parameterised by a tessellation of
199 Voronoi cells, which adapt throughout the inversion to the spatially variable data coverage.
200 The parameterisation is thus transdimensional in that the number, position, size and velocities
201 of the cells are unknowns in the inversion and are implicitly controlled by the data. The
202 approach is also considered hierarchical since the level of noise is treated as an unknown in
203 the inversion process (Bodin et al., 2012). The final results of the inversion are represented by
204 probability density functions with the average representing our “preferred” model and the
205 standard deviation a measure of uncertainty.

206 With the set of period-dependent group velocity maps from the first stage of the
207 inversion (Supplementary Fig. 5), we extracted velocity values at a regular grid of points
208 across the study area in order to generate pseudo 1D group velocity dispersion curves at ~25
209 km spacing. These 2,903 curves were then independently inverted for 1D shear-wave velocity
210 models by using a similar transdimensional, hierarchical Bayesian technique as described
211 above, and subsequently merged together to create a full 3D model. The uncertainty estimates
212 for the 2D group velocity maps were used to weight the input dispersion data in the 1D
213 inversions. This ensures that noisy measurements (i.e. large standard deviation values) will
214 not unduly influence the final solution. The average and standard deviation of each 1D model
215 was used to construct the final 3D solution model and its associated uncertainty.

216

217 **2.5. Solution quality and synthetic resolution tests**

218 To assess the reliability of group velocity maps produced by the 2D Bayesian
219 inversion method, we performed a series of resolution tests based on synthetic data. In order
220 to illustrate the potential recovery of velocity discontinuities and structure at different scales,
221 we applied the so-called synthetic “checkerboard test”. This involved using an identical
222 source-receiver path configuration to the observational dataset to predict travel-time residuals
223 for a predetermined checkerboard structure defined by a pattern of alternating high and low
224 velocity anomalies. Here, we assessed three checkerboard sizes: small (2.5°x1.5°); medium

225(4.0°x2.5°); and large (5.5°x3.5°), with maximum perturbations of the synthetic velocity
226anomalies of ± 0.5 km/s. Gaussian noise with a standard deviation equal to 1 s was added to
227the synthetic data to simulate uncertainties associated with the observational dataset (e.g.
228picking of group arrival time as a function of period). We used identical source–receiver path
229combinations to the observational dataset at 10, 20 and 30 s periods; the input structure for
230each of the three checkerboard sizes are shown in Fig. 3 (left column). The inversion was
231then carried out using the transdimensional, hierarchical Bayesian scheme.

232 The quality of the recovered checkerboard pattern is generally good (Fig. 3), with
233reasonable recovery of the input amplitudes. Smearing of the velocity model is evident in
234some places, particularly in regions peripheral to the bounds of the receiver array. For
235example, the poor resolution in the north-western corner of the array is due to the station
236configuration, with only a single isolated receiver on the Faroe Islands that is somewhat
237removed from the rest of the array. However, across the North Sea itself there is some
238smearing in both NW-SE and NE-SW directions, but the distortion it causes is not severe.
239Overall, the checkerboard tests demonstrated that data from the 54 stations used in this work
240are capable of resolving features ~ 170 km in size with even better recovery in regions of the
241model with concentrated path coverage where we might expect smaller features to be better
242resolved (Fig. 3).

243 In order to investigate the reliability of the second stage of the transdimensional,
244hierarchical, Bayesian inversion, in which pseudo-group-velocity dispersion curves are
245inverted for 1D shear velocity models, we performed another synthetic test. A four-layer
246crustal shear wave velocity model which includes a low velocity layer was used as the
247synthetic input to test the ability of the inversion to recover structure, with Gaussian noise of
2480.2 km/s standard deviation added to the group dispersion data to simulate measurement
249uncertainty. The quality of the recovered 1D shear velocity model is generally good; the
250probability density plot and its mean are in approximate agreement with the input model
251(Supplementary Fig. 6), although the largest inconsistencies between the synthetic and
252recovered model occur in the neighbourhood of the velocity discontinuities. Given that
253surface waves cannot discriminate between velocity discontinuities and strong velocity
254gradients, the fact that the mean solution model produces a smoothed version of the layered
255input model is to be expected.

256

2573. Results

258 We present the 3D crustal structure beneath the North Sea region in a series of
259 horizontal and vertical slices taken from the final tomographic solution. Significant velocity
260 anomalies that will be interpreted later are numbered on the horizontal slices in Fig. 4. We
261 use the standard deviation of the model ensemble, computed at each individual grid point in
262 latitude, longitude and depth, as an estimate of uncertainty (Fig. 5). Regions of high standard
263 deviation can generally be correlated with a lack of path coverage or lack of crossing paths.
264 Because there are no seismic stations beneath the oceans, uncertainty is naturally higher
265 offshore compared to onshore.

266 Fig. 4(a) shows a horizontal slice at 4 km depth, which is dominated by low shear-
267 wave velocities across the North Sea. These velocities, which vary between 2.2 and 2.9 km/s,
268 are widespread across northern Germany, the Netherlands, Denmark and through the Central
269 North Sea towards and beyond Shetland and Norway (labelled '1'). A notable area of higher
270 velocity between the lows in the North Sea is a region with velocities of ~ 3.5 km/s to the east
271 of northern England (labelled '2'). At 8 and 11 km depths (Fig. 4b-c), velocities of 2.8-3.1
272 km/s span much of the North Sea between the UK and Denmark. This relatively low velocity
273 structure appears to terminate at the UK coastline, but may extend onshore in the east across
274 northernmost Germany (labelled '3'). The horizontal slice at 15 km depth (Fig. 4d) also
275 shows the low velocity anomaly, but here it is confined to the western part of the North Sea,
276 adjacent to the UK. This implies that the anomaly could be thicker and/or dipping westward.
277 At the eastern end of the depth slices at 11 and 15 km depth (Figs. 4c-d) is an area of elevated
278 velocity in the vicinity of Denmark and southern Sweden (labelled '4'). It is characterised by
279 velocities of ~ 4.1 km/s compared to its surroundings of ~ 3.8 km/s. Fig. 4(d-f) shows
280 horizontal slices at 15, 20 and 25 km depth, on which we observe a pronounced zone of
281 velocities > 4.1 km/s that extend and widen northwards from the centre of the North Sea
282 (labelled '5'). This zone is generally surrounded by lower velocities of ~ 3.5 - 3.8 km/s. At 25
283 km depth (Fig. 4f), this high velocity region appears to widen south of the centre of the North
284 Sea; for example, at $\sim 56^\circ$ N it widens from ~ 170 km at 20 km depth, to ~ 360 km at 25 km
285 depth. This widening is greater in the west of the velocity anomaly than the east. It also
286 broadens with depth further north, where at 59° N the elevated velocities extend from 215 km
287 wide at 20 km depth, to 295 km wide at 25 km depth. At depths of 20 and 25 km (Fig. 4e-f) a
288 second region of very high velocities (> 4.1 km/s) is present below northern Germany
289 (labelled '6'). There appears to be a connection between the high velocities in the northern
290 and central North Sea and those below northern Germany in a narrow (~ 100 km) \sim N-S
291 trending zone which features velocities of ~ 4.2 km/s.

292 Fig. 6(a) shows a vertical slice through our 3D shear velocity model taken at 60°
293 latitude, which extends from the west of Shetland to eastern Norway. Assuming crustal
294 velocities are generally <4.2 km/s (Kennett et al., 1995), we observe thin (~14 km) crust
295 below the Viking Graben. Overlying the thinnest sections of crust, low velocities (<2.7 km/s)
296 span the North Sea upper crust from Shetland to Norway (anomaly '1'). We also observe that
297 the crustal velocity character is significantly different on either side of the thin region. Below
298 Norway, crustal thickness is likely to be >30 km whereas below the Shetland Plateau it is ~27
299 km. Furthermore, on the Norwegian side the velocity properties are apparently more uniform
300 with higher velocities (mostly >3.4 km/s) throughout, whereas on the Shetland side lower
301 velocities are more extensive (~3.0 km/s in the upper crust). A vertical slice through our
302 shear velocity model further south at 56° N (Fig. 6c) highlights other significant features in
303 our results. Again, assuming a base of crust velocity of 4.2 km/s, we observe that the crustal
304 thickness below central Scotland is ~30 km, which is in contrast to Denmark and Sweden
305 where mantle velocities are not reached, implying a crustal thickness of >30 km. Low
306 velocity anomaly '3' is visible below the North Sea on this vertical slice. These velocities are
307 lower than anywhere else in our model at these depths. This low velocity anomaly has an
308 apparent westward dip or alternatively thickens to the west but does not continue below
309 Scotland. The final key feature to note in this cross-section is the asymmetry of the highly
310 elevated mantle velocities (>4.3 km/s, labelled '5'), which underlie the thin crust below the
311 North Sea (Fig. 6a,c). We observe that these high velocities have a much more abrupt
312 transition to normal crustal velocities in the east compared with the more gradual transition
313 on the Scottish side.

314

315 4. Discussion

316 In this section we focus on key features in the new 3D shear-wave velocity model that
317 are relevant in addressing the link between lithospheric extension and pre-existing structures,
318 which is the main goal of this study.

319

320 4.1. Upper Crust

321 In the uppermost crust, shear-wave velocities of 2.2-2.9 km/s are widespread across
322 northern Germany, the Netherlands, Denmark and throughout the North Sea (labelled '1' on
323 Fig. 4a). These low velocities are characteristic of sedimentary basins and we find their
324 distribution matches well with sediment thickness maps such as EuCRUST-07 (Tesauro et
325 al., 2008), which is derived from seismic reflection, refraction and receiver function data.

326 However, there is one notable region of significant discrepancy between EuCRUST07 and
327 our model in the vicinity of the Mid North Sea High. Here, a distinct area of higher velocity
328 (~3.5 km/s) is observed on the 4 km depth slice (anomaly '2'; Fig. 4a & 6c), which extends
329 from the northeast coast of England and across the Mid North Sea High region (Fig. 1), and
330 appears to be confined to the uppermost ~5 km of crust (Fig. 6c). The Mid North Sea High
331 lies in the Central North Sea, between the Northern and Southern Permian Basins. Gravity
332 studies have been used to map the presence of granites across the area (Wernicke, 1985) and
333 Well 37/25-1 (drilled in 2009 by Esso) penetrated the Dogger High, and found that the crustal
334 blocks likely contain granite cores. These blocks acted as relative highs since at least
335 Devonian times, as shown by a good match with the thickness of the Carboniferous and
336 Devonian sedimentary deposits, where thinner sections represent basement highs at the time
337 of deposition (e.g. Arsenikos et al., 2019). These intrusive igneous bodies likely exhibit
338 higher shear-wave velocities than the surrounding sedimentary basins. Increasingly, evidence
339 shows that shallow-level crustal intrusions are emplaced and grow through the incremental
340 stacking of sill-like sheets, rather than isolated plutons (e.g. Wilson et al., 2016). The
341 presence of granite throughout the MNSH uppermost crust is therefore a plausible
342 explanation for the elevated velocities in this region. The size of each individual granite
343 pluton is likely well below the resolving power of our dataset, which would help explain why
344 we observe a diffuse zone of elevated wavespeed (Fig. 3). Another consideration is that
345 several boreholes on the MNSH found sedimentary rocks which experienced greenschist and
346 possibly amphibolite facies metamorphism in the late Ordovician (Pharaoh et al., 1995). The
347 laboratory estimated shear-wave velocity of greenschist is 3.57 km/s (Christensen, 1996),
348 which is very close to the ~3.5 km/s shear-wave velocity we find in our model. It is therefore
349 possible that a combination of granite-cored fault blocks and greenschist facies is why we
350 observe widespread elevated velocities in the upper crust around the MNSH.

351

352 4.2. Low velocities in the mid-crust

353 A significant volume of unexpectedly low velocities (2.8-3.1 km/s) spans much of the
354 North Sea between Denmark and the UK adjacent to the Viking and Central Grabens, best
355 identified on the 11 km depth slice (anomaly '3'; Fig. 4c). This relatively low velocity zone
356 appears to terminate at the eastern UK coastline and is also present on the horizontal model
357 slice at 15 km depth (Fig. 4d), where it is confined to the western part of the North Sea. On
358 cross-section slice B-B' (Fig. 6c) anomaly '3' apparently extends to ~16 km depth, below
359 which highly elevated velocities of >4.1 km/s exist, most likely indicating moderately

360thinned crust below it. Finding an unequivocal interpretation of this anomaly is challenging
361because it is situated entirely offshore and at depths of >10 km where no boreholes penetrate.
362We observe relatively higher standard deviation values (therefore greater uncertainty) in the
363offshore area, where anomaly '3' is located, than for the onshore area (Fig. 5c-d) and the
364checkerboard resolution tests show that anomalies the size of '3' can be subject to a degree of
365smearing (Fig. 3e-h). Furthermore, our study is based on Rayleigh waves, which are sensitive
366to vertically polarised shear wave speeds (V_{SV}) that may be slower than horizontally
367polarised shear speeds (V_{SH}). We can therefore only make tentative assumptions about
368anisotropy in the region.

369 If the low velocities are caused by sedimentary rocks, they would likely be Devonian
370age or older (Arsenikos et al., 2019; Milton-Worsell et al., 2010). However, at depths of up
371to 16 km, sedimentary material is unlikely to remain un-metamorphosed by high pressures
372and temperatures. Assuming an average geotherm of 23°C/km (Madsen, 1974), the
373temperature at 15 km depth would be ~345 °C putting the rocks firmly in the greenschist
374metamorphic facies zone (Yardley, 1989). The laboratory estimated shear-wave velocity of
375greenschist is 3.57 km/s (Christensen, 1996), making it an unlikely candidate for our low
376shear-wave velocity zone (2.8-3.1 km/s).

377 A number of deep seismic reflection profiles acquired across the North Sea in the
3781980s (BIRPS and SNST83-7; Klemperer et al., 1991) show a markedly unreflective upper-
379to mid-crust in the same region as our anomaly '3', and (in most cases) it occurs directly
380above highly reflective crust. The high reflectivity itself has been attributed to magmatic
381underplating, which has been invoked by a number of authors to explain thick (>10 km)
382high-velocity layers with/or strong horizontal reflectivity in the lower crust (e.g. Thybo et al.,
3832000). Low shear wave velocity regions with corresponding unreflective crustal character are
384located above the strongly reflective layer and could therefore be related to possible
385magmatic underplating in the lower crust. For example, by comparing our findings for
386anomaly '3' to the present-day Rhine Graben, we hypothesise that the same process of
387magmatic underplating followed by expulsion of water from the metamorphosed intrusions
388has occurred in both locations (Wenzel and Sandmeier, 1992). It is possible that extra fluids
389trapped in the mid- to upper crust as a result of dehydration reactions are contributing to the
390unusually low wavespeeds below the North Sea. The low shear-wave velocity zone in our
391model is characterised by velocities of 2.8-3.1 km/s, and corresponds to low P-wave
392velocities of 6.3-6.4 km/s in part of the same region (Smit et al., 2016). Taking averages, this
393gives a V_P/V_S ratio of approximately 2.2, i.e. higher than normal. Wang et al. (2012) showed

394in laboratory experiments that V_P/V_S remained high and close to 2.2, even at seismic
395frequencies, in samples with low aspect ratio microcracks saturated with incompressible fluid
396and high pore fluid pressure. The implication for our study is that the presence of fluid and
397microcracks may be contributing to the low shear-wave velocity zone. Additionally, the
398presence of brines in microcracks and fractures have been proven to exist to depths of at least
39912 km at 190 °C and 9 km at 265 °C in the Kola (Russia) and KTB (Germany) boreholes
400respectively, where the presence of fluids correlated with and helped explain the lowered
401seismic velocities (Smithson et al., 2000). Furthermore, as part of their simple shear model
402for extension, Lister et al. (1991) predicted underplating to occur in the crust on the opposite
403side of the detachment zone to the main sedimentary basin formation. In our new model, we
404see similar asymmetric geometries characteristic of this simple shear model in the central and
405southern North Sea (e.g. Fig. 6c), whereby the low shear-wave velocity zone and associated
406highly reflective lower crust is offset from the sedimentary basin. Moreover, the higher than
407normal V_P/V_S we observe may be an effect of serpentinisation (e.g. Christensen, 1996; Ji et
408al., 2013), which could have formed due to fluid influx caused by dehydration of underplated
409material.

410 An alternative end-member idea for interpretation of the mid-crustal low velocity
411zone expands on a hypothesis recently presented by Smit et al. (2016). They identified a low
412(6.3-6.4 km/s) P-wave velocity zone in the mid- to lower crust along the Caledonian Thor
413suture zone on a number of deep seismic reflection and refraction profiles including MONA
414LISA (profiles 1–3) across the Central Graben, combined European GeoTraverse sub-profiles
415EUGEMI and EUGENO-S 1, and LT-7, PQ-2 and BASIN-9601 profiles across the Baltica
416margin. The low velocity zone is identified consistently across these profiles, but they are too
417short to image its westward extent. We find that our model exhibits low S-wave velocities in
418the same location as the low P-wave anomalies found in Smit et al. (2016); however, the
419match is not perfect and the low V_S region extends much further west than the low V_P region.
420Based on the distribution of low V_S in our model, we propose that the low velocity zone
421continues much further westwards and reaches the British coastline. The low P-wave
422velocities were interpreted by Smit et al. (2016) as a separate crustal unit consisting of a
423collapsed Caledonian accretionary complex located between Baltica and Avalonia, who also
424compare it to the present-day Kuril and Cascadia subduction zones. In these modern cases,
425broad zones of low (6.4-6.6 km/s) P-wave velocities have been found in the subduction
426channels and Ramachandran et al. (2006) interpreted the low velocities at Cascadia to be due
427to either trapped fluids, highly sheared lower crustal rocks, and/or underthrust accretionary

428rock. Furthermore, tomographic studies of the Nankai and Cascadia subduction zones have
429confirmed the presence high V_P/V_S (>2.1) (Audet et al., 2009; Kodaira, 2004), similar to what
430we infer from our model. These zones have been interpreted as regions of high pore fluid
431pressure (Kodaira, 2004; Peacock et al., 2011) and where they also exhibit low velocities they
432may be due to strong mineral preferred orientation, of serpentine in particular (Bezacier et al.,
4332010). The Caledonian Orogeny involved the subduction of part of the Tornquist Sea basin
434beneath Avalonia (Pharaoh et al., 1995), and geophysical evidence suggests that at least two
435subduction zones were involved in this process, remnants of which are presently known as
436the Thor Suture and the Dowsing-South Hewett Fault Zone. This fault zone is a long-lived
437NW-SE trending crustal lineament (Fig. 1) and was reactivated throughout late Palaeozoic
438and Mesozoic times (Pharaoh, 1999). On deep seismic reflection data it separates crust of
439distinctly different seismic reflectivity character, and a dipping reflector at the Moho and
440upper mantle has been mapped parallel to, and just coastward of the fault zone which may
441mark the location of an Ordovician subduction zone and/or crustal suture (Klemperer et al.,
4421991). The low velocity zone in our shear-wave velocity model apparently terminates at the
443Dowsing-South Hewett Fault Zone (within our resolution limits) and therefore it is plausible
444that the low velocity region (anomaly '3') is either constrained or caused by these two ancient
445subduction zones (Thor and Dowsing-South Hewett).

446

447**4.3. Failed rift – thinned crust**

448 One of the most striking features of the 3D shear-wave velocity model is a high
449velocity zone (>4.3 km/s) that is constrained at ~ 15 km depth beneath the northern North Sea
450(Fig. 4d) and extends southward into the central North Sea where it occurs at ~ 20 km depth
451(Fig. 4e). These high velocities are likely to be the result of surface waves sampling the
452uppermost mantle, which can be defined seismically as shear-wave speeds >4.3 km/s (e.g.
453PREM; Dziewonski and Anderson, 1981; AK135; Kennett et al., 1995). Labelled as velocity
454anomaly '5', the high velocity zone exhibits apparent asymmetry that can be clearly observed
455on cross-section B-B' (Fig. 6c) with a more abrupt transition to lower velocities in the east,
456compared with a more gradual, dipping geometry in the west. This asymmetry is similar to
457that proposed to explain lithospheric extension by the simple shear model (Wernicke, 1985),
458and its prediction of a sedimentary basin that is laterally offset from the melting caused by
459uprising asthenosphere, and an apparent sloping geometry of the thinned crust, matches what
460we observe in our model (Fig. 6c). Whilst the resolution of our ambient seismic noise
461tomography model is not sufficient to detect any lithosphere-scale detachment fault zone, it is

462also possible that such a large-scale shear zone cutting the lithosphere does not exist (e.g.
463Yamasaki and Gernigon, 2009).

464 The asymmetric thin crust in the central and southern North Sea is markedly different
465from the shape of the fast anomaly further north, as shown on cross-section A-A' (Fig. 6a),
466where it appears to be more symmetric. This is in agreement with Klempere (1988), who
467found no evidence for the existence of lithosphere-penetrating low-angle detachments (i.e.
468zones of simple shear; Wernicke, 1985) on NSDP deep seismic reflection profiles in the
469northern North Sea, and suggested pure shear (i.e. symmetric; McKenzie, 1978) acted during
470extension in this location.

471 In our velocity model, anomaly '5' lies directly below the location of the Viking and
472Central Grabens (Fig. 1). It therefore appears reasonable to claim that we constrain, for the
473first time at this scale, significant changes in geometry along strike of the thinned crust of the
474North Sea rift system. The high velocity anomaly appears to narrow towards the southern
475North Sea, reflecting the propagation of rifting activity that initially commenced during
476earliest Triassic times in the Norwegian-Greenland Sea area and propagated southward
477during Jurassic times into the central and southern North Sea (Ziegler, 1990). The symmetric
478rifting in the northern North Sea is in contrast to the asymmetric rifting in the central and
479southern North Sea, with the different styles most likely controlled by ancient paleo-
480continents in each location; i.e. extension in lithosphere of Baltica and Laurentia origin in the
481north led to symmetric rifting, while extension in lithosphere of Avalonia and Laurentia
482origin in the south resulted in asymmetric rifting and eventual termination of the North Sea
483failed rift system (see Fig. 7 for a schematic interpretation of the two rifting styles).

484 At depths >20 km, a second region of very high velocities (>4.3 km/s) is present
485below northern Germany (anomaly '6'; Fig. 2f). At shallower depths, this is the approximate
486location of the late Jurassic to early Cretaceous age Lower Saxony Basin (Fig. 1). The
487elevated velocities that characterise anomaly '6' are very similar to those of anomaly '5',
488perhaps indicating that this is another area of thinned crust where mantle velocities are being
489sampled. Interestingly, there appears to be some connection between the fast velocities below
490the Central Graben and those below the Lower Saxony Basin in a narrow (~100 km wide)
491zone of ~N-S trending velocities of ~4.2 km/s (Fig. 4e-f). This zone is situated beneath the
492South-Central North Sea Graben and the eastern Netherlands, both areas of substantial
493Carboniferous-Jurassic igneous activity which was coincident with the initial development of
494the Proto-South Central North Sea Graben (Sissingh, 2004). Taking into consideration the
495resolution of our model (Fig. 3), we tentatively suggest that the spatial relationship between

496the igneous activity and elevated shear-wave velocity zone could indicate that we are
497observing the extension of the southernmost part of the North Sea failed rift system into
498northern Germany.

499

5004.4. Failed rift systems and structural inheritance

501 Structural inheritance is a property of the continental lithosphere that focuses
502deformation along pre-existing structures, e.g. faults, shear or suture zones (e.g. Schiffer et
503al., 2019). The associated reactivation is primarily controlled by the compositional and
504mechanical properties of the pre-existing structures (e.g. Holdsworth et al., 2001). In relation
505to the distribution of paleo-plates in the North Sea, rifting appears to initially follow the path
506of least resistance, the weakness that was the suture zone between Laurentia and Baltica, in a
507symmetric fashion, evidenced by our new 3D velocity model. When it reached the triple plate
508collision junction, it changes rifting style, becoming strongly asymmetric (Fig. 7). Our new
509model shows that the rift was unable continue to propagate very far into Avalonian
510lithosphere, likely because it possesses different mechanical properties that require greater
511tectonic forces to extend.

512 Similarly, during Jurassic-Cretaceous rifting of Australia and Antarctica, Bass Strait
513(separating Tasmania from mainland Australia) became a failed arm of the Southern Rift
514System. Rifting likely failed because Bass Strait is underlain by a Precambrian continental
515fragment known as the Vandieland microcontinent, which is thought to be mechanically
516stronger than the already extensively faulted strike-slip zone to the west, where the Southern
517Rift System eventually achieved full rifting when Antarctica separated from Australia (e.g.
518Gibson et al., 2012).

519 It appears that structural inheritance, and in particular the influence of paleo-plates,
520plays a key role in rifting and rift failure. For example, a rift can initially exploit the weakest
521part of the lithosphere at a paleo-suture zone. However, if a juxtaposed paleo-plate is
522mechanically stronger and hence is able to resist strain localisation, then the rift may cease to
523propagate and ultimately fail. Our results provide new evidence of how inherited lithosphere
524properties, such as suture zones and variations in mechanical strength, are a fundamental
525control on rift formation, style, propagation and termination.

526

527

5285. Conclusions

529 We present the first 3D shear-wave velocity model of the North Sea region from
530 ambient seismic noise tomography. Due to noise sources within the North Sea, previous
531 studies have found it difficult to extract reliable inter-station group velocity dispersion data.
532 However, by utilising time–frequency domain phase-weighted stacking to improve the
533 signal-to-noise, we were able to successfully extract robust surface wave dispersion
534 information. A transdimensional, hierarchical, Bayesian inversion method, which is highly
535 data driven and requires minimal tuning of initial parameters, was then applied to invert for
536 shear wave velocity. This approach accounts for heterogeneous data coverage, produces an
537 ensemble of solution models and can constrain data uncertainty parameters. Our main
538 findings include:

539

- 540 • Low velocities (<2.9 km/s) across much of the North Sea, Denmark, the
541 Netherlands and northern Germany which are interpreted as signatures of the
542 major North Sea sedimentary basins and match well with published sediment
543 thickness maps;
- 544 • Relatively higher velocities (~3.5 km/s) in the upper crust of the Mid North Sea
545 High region, typical of granites and greenschist and corresponding to locations of
546 granites mapped from gravity anomalies;
- 547 • Anomalously low velocities (2.8-3.1 km/s) in the upper- to mid-crust in the
548 vicinity of the Thor suture and across the southern North Sea, which could be
549 interpreted as representing the remnants of a Caledonian accretionary complex.
550 Alternatively, they may be caused by the presence of water (and/or microcracks)
551 related to possible magmatic underplating in the area associated with Jurassic
552 rifting in the North Sea;
- 553 • Relatively higher velocities in the vicinity of the Trans European Suture Zone
554 (~4.1 km/s compared to its surroundings of ~3.8 km/s);
- 555 • Significantly elevated velocities (>4.2 km/s) representing thinned (13-18 km)
556 crust beneath the Viking and Central Grabens. Rift style appears to be symmetric
557 in the northern North Sea Viking Graben and strongly asymmetric in the Central
558 Graben. This may be related to the location of the Laurentia-Avalonia-Baltica
559 paleo-plates.

560 • Shallow high velocities (>4.2 km/s at 20 km depth, implying thinner crust) below
561 Germany, with a tentative connection to the main North Sea rift system via a
562 narrow N-S trending corridor of high velocities.

563

564 Finally, we find that both rifting style (symmetric vs. strongly asymmetric) and
565 propagation ability varies across crust of different paleo-plate origins. We suggest that our
566 new 3D shear-wave velocity model provides evidence of how inherited paleo-plate
567 boundaries and suture zones play a fundamental role in the genesis, evolution and termination
568 of failed continental rifts.

569

570 Acknowledgments

571 The work contained in this paper was conducted during a PhD study undertaken as
572 part of the Natural Environment Research Council (NERC) Centre for Doctoral Training
573 (CDT) in Oil & Gas [grant number NEM00578X/1]. This work was performed using the
574 Maxwell High Performance Computing Cluster of the University of Aberdeen IT Service
575 (www.abdn.ac.uk/staffnet/research/hpc.php), provided by Dell Inc. and supported by Alces
576 Software. Plots were generated with the Generic Mapping Tools (GMT; (Wessel et al., 2013)).
577 We thank Nick Schofield and Tim Pharaoh for constructive conversations, which aided the
578 interpretation of our results, and Amy Gilligan for her insightful advice during preparation of
579 this manuscript.

580

581 References

Allmark, C., Curtis, A., Galetti, E., de Ridder, S., 2018. Seismic attenuation from ambient noise across the north sea Ekofisk permanent array. *Journal of Geophysical Research: Solid Earth* 123, 8691–8710.

Arsenikos, S., Quinn, M., Kimbell, G., Williamson, P., Pharaoh, T., Leslie, G., Monaghan, A., 2019. Structural development of the Devonian-Carboniferous plays of the UK North Sea. *Geological Society, London, Special Publications* 471, 65–90. <https://doi.org/10.1144/SP471.3>

Audet, P., Bostock, M.G., Christensen, N.I., Peacock, S.M., 2009. Seismic evidence for overpressured subducted oceanic crust and megathrust fault sealing. *Nature* 457, 76.

Bensen, G.D., Ritzwoller, M.H., Barmin, M.P., Levshin, A.L., Lin, F., Moschetti, M.P., Shapiro, N.M., Yang, Y., 2007. Processing seismic ambient noise data to obtain reliable

broad-band surface wave dispersion measurements. *Geophysical Journal International* 169, 1239–1260.

Bezacier, L., Reynard, B., Bass, J.D., Sanchez-Valle, C., Van de Moortèle, B., 2010. Elasticity of antigorite, seismic detection of serpentinites, and anisotropy in subduction zones. *Earth and Planetary Science Letters* 289, 198–208.

Bodin, T., Sambridge, M., Rawlinson, N., Arroucau, P., 2012. Transdimensional tomography with unknown data noise. *Geophys J Int* 189, 1536–1556. <https://doi.org/10.1111/j.1365-246X.2012.05414.x>

Christensen, N., 1996. Poisson's ratio and crustal seismology. *Journal of Geophysical Research: Solid Earth* 101, 3139–3156.

Christensen, N.I., Mooney, W.D., 1995. Seismic velocity structure and composition of the continental crust: A global view. *Journal of Geophysical Research: Solid Earth* 100, 9761–9788.

Donato, J.A., Martindale, W., Tully, M.C., 1983. Buried granites within the Mid North Sea High. *Journal of the Geological Society* 140, 825–837. <https://doi.org/10.1144/gsjgs.140.5.0825>

Dziewonski, A.M., Anderson, D.L., 1981. Preliminary reference Earth model. *Physics of the earth and planetary interiors* 25, 297–356.

Galetti, E., Curtis, A., Baptie, B., Jenkins, D., Nicolson, H., 2016. Transdimensional Love-wave tomography of the British Isles and shear-velocity structure of the East Irish Sea Basin from ambient-noise interferometry. *Geophysical Journal International* 208, 36–58.

Gibson, G.M., Totterdell, J., Morse, M.P., Goncharov, A., Mitchell, C.H., Stacey, A.R., 2012. Basement Structure and Its Influence on the Pattern and Geometry of Continental Rifting and Breakup Along Australia's Southern Rift Margin. *Geoscience Australia*.

Herrmann, R.B., 2013. Computer programs in seismology: An evolving tool for instruction and research. *Seismological Research Letters* 84, 1081–1088.

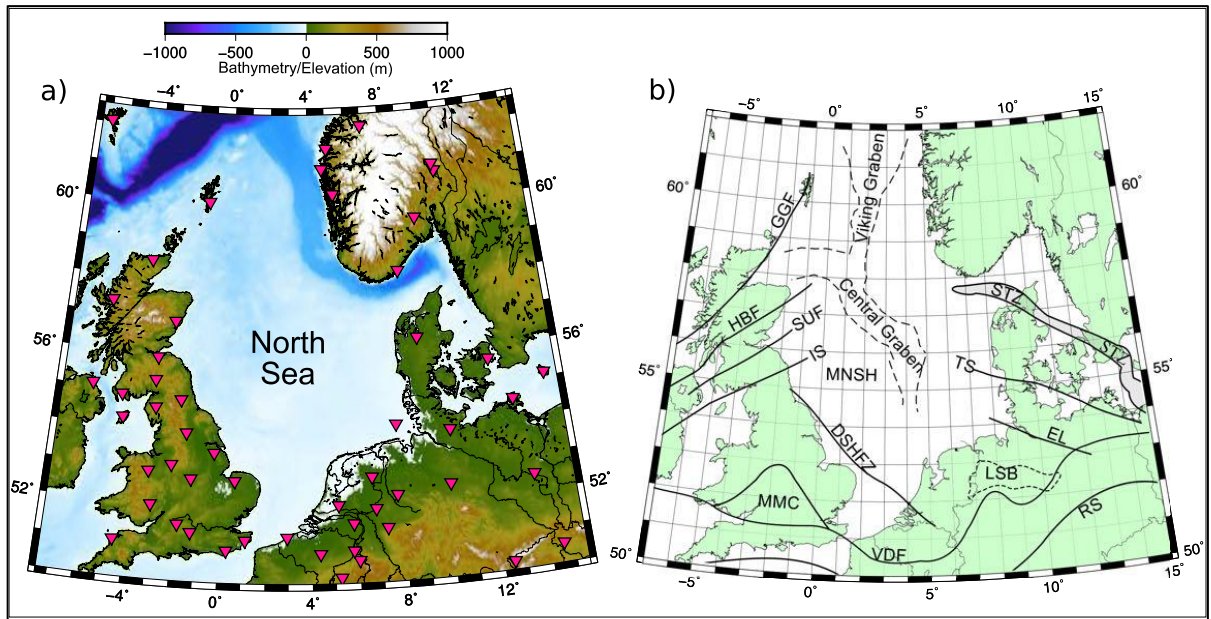
Holdsworth, R.E., Stewart, M., Imber, J., Strachan, R.A., 2001. The structure and rheological evolution of reactivated continental fault zones: a review and case study. *Geological Society, London, Special Publications* 184, 115–137.

Ji, S., Li, A., Wang, Q., Long, C., Wang, H., Marcotte, D., Salisbury, M., 2013. Seismic velocities, anisotropy, and shear-wave splitting of antigorite serpentinites and tectonic implications for subduction zones. *Journal of Geophysical Research: Solid Earth* 118, 1015–1037.

- Kennett, B.L., Engdahl, E.R., Buland, R., 1995. Constraints on seismic velocities in the Earth from traveltimes. *Geophysical Journal International* 122, 108–124.
- Klemperer, S.L., 1988. Crustal thinning and nature of extension in the northern North Sea from deep seismic reflection profiling. *Tectonics* 7, 803–821.
- Klemperer, S.L., Hobbs, R., Hobbs, R.W., 1991. *The BIRPS Atlas: Deep Seismic Reflections Profiles Around the British Isles*. Cambridge University Press.
- Kodaira, S., 2004. High Pore Fluid Pressure May Cause Silent Slip in the Nankai Trough. *Science* 304, 1295–1298. <https://doi.org/10.1126/science.1096535>
- Lecocq, T., Caudron, C., Brenguier, F., 2014. MSNoise, a python package for monitoring seismic velocity changes using ambient seismic noise. *Seismological Research Letters* 85, 715–726.
- Lister, G.S., Etheridge, M.A., Symonds, P.A., 1991. Detachment models for the formation of passive continental margins. *Tectonics* 10, 1038–1064.
- Madsen, L., 1974. Approximate geothermal gradients in Denmark and the Danish North Sea sector. *Danm. Geol. Unders. \AArbog for* 5–16.
- McKenzie, D., 1978. Some remarks on the development of sedimentary basins. *Earth and Planetary science letters* 40, 25–32.
- Milton-Worsell, R., Smith, K., McGrandle, A., Watson, J., Cameron, D., 2010. The search for a Carboniferous petroleum system beneath the Central North Sea. *Petroleum Geology Conference series* 7, 57–75. <https://doi.org/10.1144/0070057>
- Nicolson, H., Curtis, A., Baptie, B., 2014. Rayleigh wave tomography of the British Isles from ambient seismic noise. *Geophysical Journal International* 198, 637–655.
- Peacock, S.M., Christensen, N.I., Bostock, M.G., Audet, P., 2011a. High pore pressures and porosity at 35 km depth in the Cascadia subduction zone. *Geology* 39, 471–474.
- Peacock, S.M., Christensen, N.I., Bostock, M.G., Audet, P., 2011b. High pore pressures and porosity at 35 km depth in the Cascadia subduction zone. *Geology* 39, 471–474.
- Pharaoh, T., England, R., Lee, M., 1995. The concealed Caledonide basement of Eastern England and the southern North Sea — A review. *Stud Geophys Geod* 39, 330–346. <https://doi.org/10.1007/BF02295826>
- Pharaoh, T.C., 1999. Palaeozoic terranes and their lithospheric boundaries within the Trans-European Suture Zone (TESZ): a review. *Tectonophysics* 314, 17–41. [https://doi.org/10.1016/S0040-1951\(99\)00235-8](https://doi.org/10.1016/S0040-1951(99)00235-8)

- Ramachandran, K., Hyndman, R.D., Brocher, T.M., 2006. Regional P-wave velocity structure of the Northern Cascadia Subduction Zone. *J. Geophys. Res.* 111, n/a-n/a. <https://doi.org/10.1029/2005JB004108>
- Sano, O., Kudo, Y., Mizuta, Y., 1992. Experimental determination of elastic constants of Oshima granite, Barre granite, and Chelmsford granite. *Journal of Geophysical Research: Solid Earth* 97, 3367–3379.
- Schiffer, C., Doré, A.G., Foulger, G.R., Franke, D., Gernigon, L., Holdsworth, B., Kusznir, N., Lundin, E., Peace, A., Petersen, K.D., Phillips, T., Stephenson, R., Stoker, M.S., Welford, K., 2019. Structural inheritance in the North Atlantic 81.
- Schimmel, M., Stutzmann, E., Gallart, J., 2011. Using instantaneous phase coherence for signal extraction from ambient noise data at a local to a global scale. *Geophysical Journal International* 184, 494–506.
- Sissingh, W., 2004. Palaeozoic and Mesozoic igneous activity in the Netherlands: a tectonomagmatic review. *Netherlands Journal of Geosciences* 83, 113–134.
- Smit, J., van Wees, J.D., Cloetingh, S., 2016. The Thor suture zone: From subduction to intraplate basin setting. *Geology* 44, 707–710. <https://doi.org/10.1130/G37958.1>
- Smithson, S.B., Wenzel, F., Ganchin, Y.V., Morozov, I.B., 2000. Seismic results at Kola and KTB deep scientific boreholes: velocities, reflections, fluids, and crustal composition. *Tectonophysics* 329, 301–317.
- Tesauro, M., Kaban, M.K., Cloetingh, S.A., 2008. EuCRUST-07: A new reference model for the European crust. *Geophysical Research Letters* 35.
- Thybo, H., Maguire, P.K.H., Birt, C., Perchuc, E., 2000. Seismic reflectivity and magmatic underplating beneath the Kenya Rift. *Geophysical Research Letters* 27, 2745–2748.
- Torsvik, T.H., Rehnström, E.F., 2003. The Tornquist Sea and Baltica–Avalonia docking. *Tectonophysics* 362, 67–82.
- Ventosa, S., Schimmel, M., Stutzmann, E., 2017. Extracting surface waves, hum and normal modes: time-scale phase-weighted stack and beyond. *Geophysical Journal International* 211, 30–44.
- Wang, X.-Q., Schubnel, A., Fortin, J., David, E.C., Guéguen, Y., Ge, H.-K., 2012. High V_p/V_s ratio: Saturated cracks or anisotropy effects? *Geophysical Research Letters* 39. <https://doi.org/10.1029/2012GL051742>
- Wenzel, F., Sandmeier, K.-J., 1992. Geophysical evidence for fluids in the crust beneath the Black Forest, SW Germany. *Earth-Science Reviews* 32, 61–75.

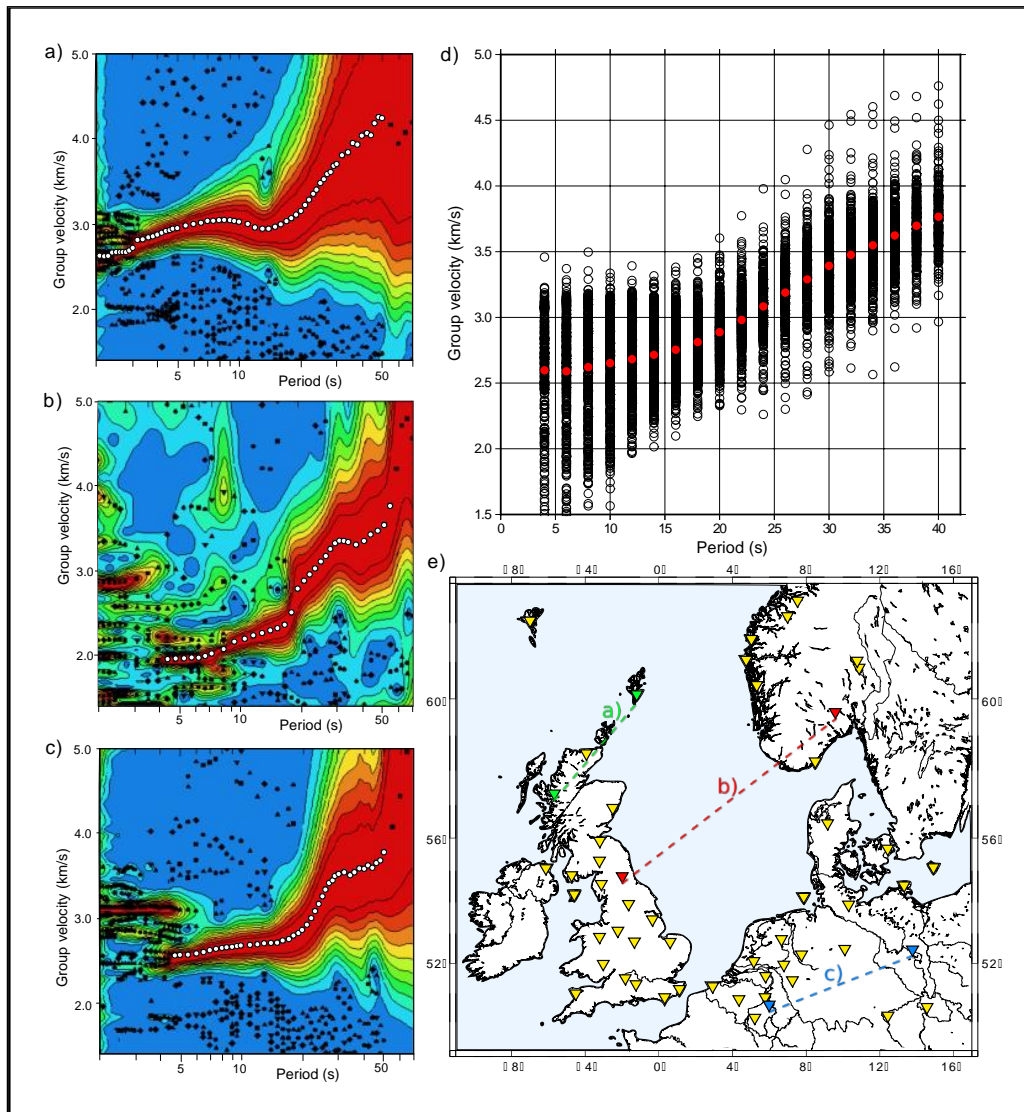
- Wernicke, B., 1985. Uniform-sense normal simple shear of the continental lithosphere. *Canadian Journal of Earth Sciences* 22, 108–125.
- Wessel, P., Smith, W.H., Scharroo, R., Luis, J., Wobbe, F., 2013. Generic mapping tools: improved version released. *Eos, Transactions American Geophysical Union* 94, 409–410.
- Wilson, P.I.R., McCaffrey, K.J.W., Wilson, R.W., Jarvis, I., Holdsworth, R.E., 2016. Deformation structures associated with the Trachyte Mesa intrusion, Henry Mountains, Utah: Implications for sill and laccolith emplacement mechanisms. *Journal of Structural Geology* 87, 30–46. <https://doi.org/10.1016/j.jsg.2016.04.001>
- Yamasaki, T., Gernigon, L., 2009. Styles of lithospheric extension controlled by underplated mafic bodies. *Tectonophysics* 468, 169–184.
- Yang, Y., Ritzwoller, M.H., Levshin, A.L., Shapiro, N.M., 2007. Ambient noise Rayleigh wave tomography across Europe. *Geophysical Journal International* 168, 259–274.
- Yardley, B.W., 1989. *An introduction to metamorphic petrology*.
- Young, M.K., Rawlinson, N., Arroucau, P., Reading, A.M., Tkalčić, H., 2011. High-frequency ambient noise tomography of southeast Australia: New constraints on Tasmania's tectonic past. *Geophysical Research Letters* 38. <https://doi.org/10.1029/2011GL047971>
- Young, M.K., Rawlinson, N., Bodin, T., 2013. Transdimensional inversion of ambient seismic noise for 3D shear velocity structure of the Tasmanian crust. *Geophysics* 78, WB49–WB62.
- Ziegler, P.A., 1990. *Geological atlas of western and central Europe*. Geological Society of London.



582
 583
 584 **Fig. 1:** Map of the North Sea and surrounding regions showing (a) seismometers used in this study (red
 585 triangles); and (b) major crustal features in the study area. GGF: Great Glen Fault; HBF: Highland Boundary
 586 Fault; SUF: Southern Uplands Fault; IS: Iapetus Suture; MNSH: Mid-North Sea High; DSHFZ: Dowsing South
 587 Hewett Fault Zone; MMC: Midlands Micro-craton; VDF: Variscan Deformation Front; LSB: Lower Saxony
 588 Basin; RS: Rheic Suture; EL: Elbe Lineament; TS: Thor Suture; STZ: Sorgenfrei-Tornquist Zone.

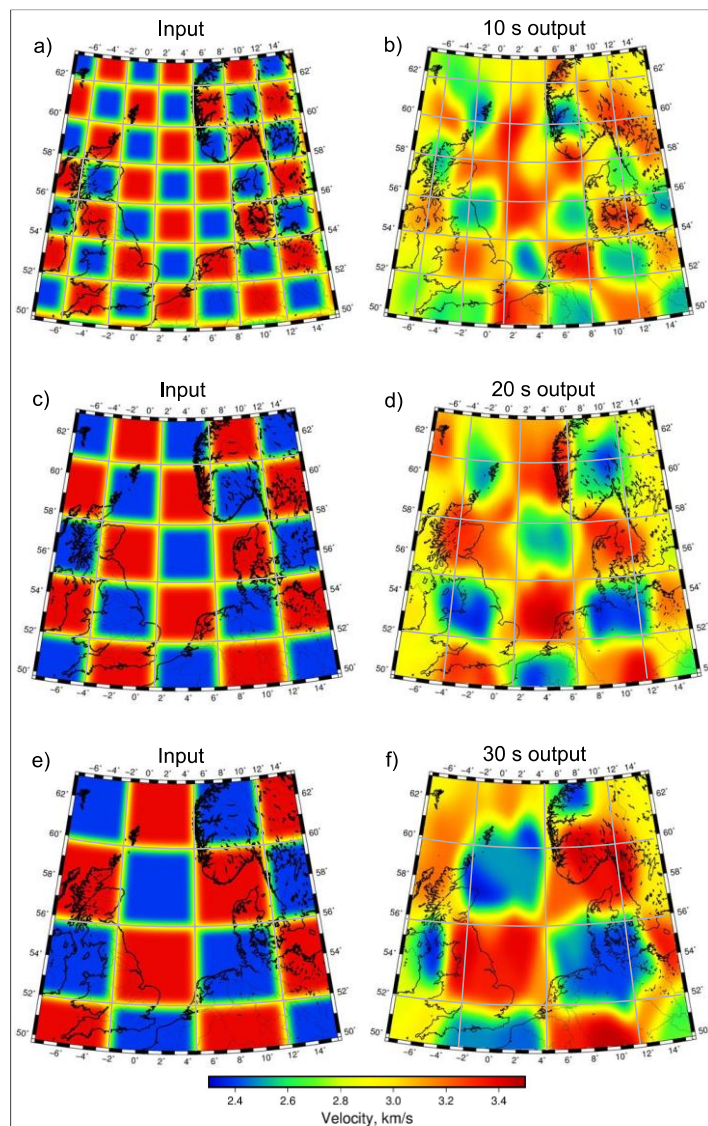
589
 590
 591
 592
 593
 594
 595
 596
 597
 598
 599
 600
 601
 602
 603
 604
 605
 606
 607
 608
 609
 610
 611
 612
 613

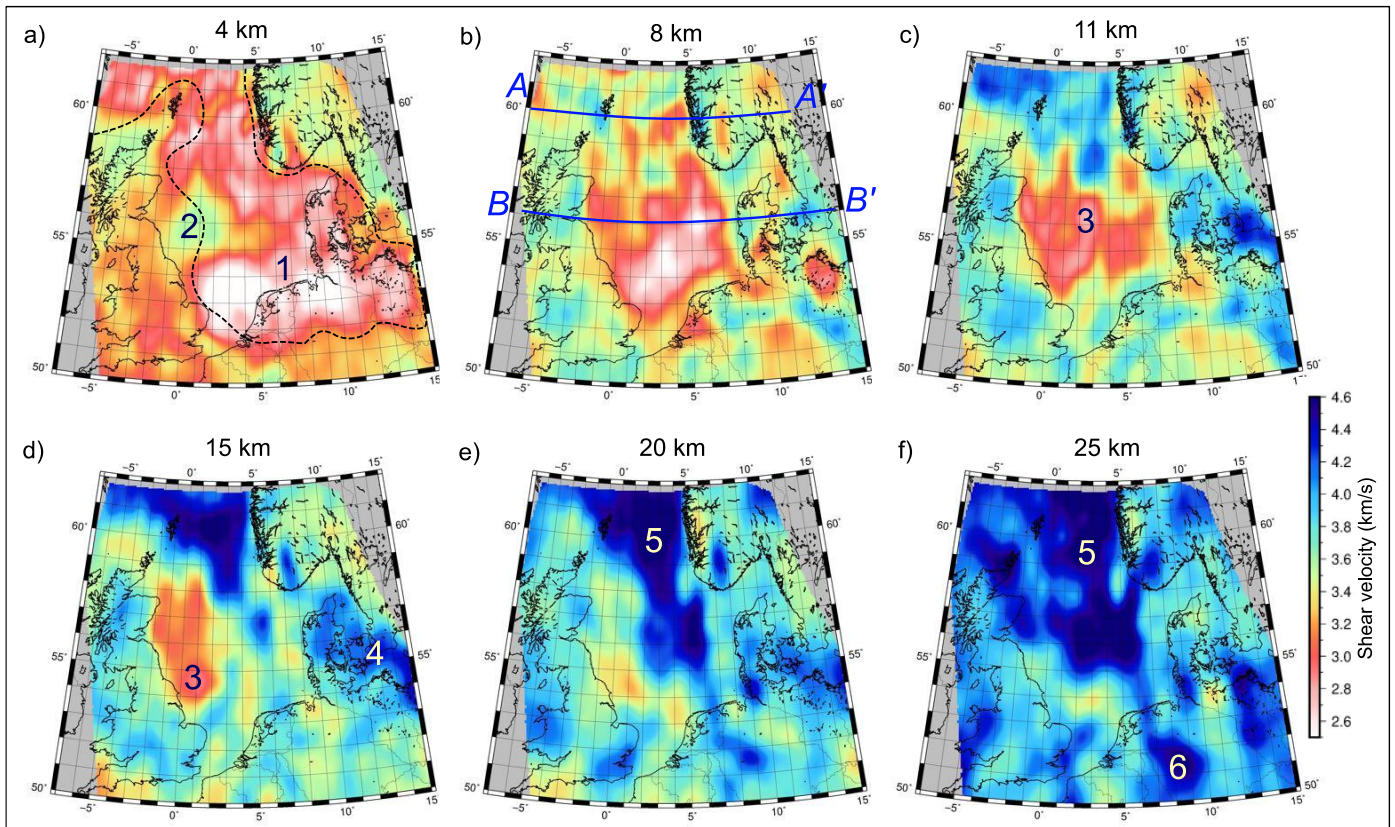
614
615
616
617
618
619
620
621
622
623
624
625
626
627
628
629
630
631
632
633
634
635
636
637
638
639
640
641
642
643
644
645
646
647
648
649
650
651
652
653
654
655
656
657
658
659
660
661
662
663
664
665
666
667
668
669
670
671
672
673



652**Fig. 2:** (a-c) Plots showing group velocity dispersion curves computed from cross-correlations between the three
653station pairs shown in (e), with white dots denoting the group dispersion picks; (d) dispersion data from all
654“good” curves, with the average for each period shown in red.

674
675
676
677
678
679
680
681
682
683
684
685
686
687
688
689
690
691
692
693
694
695
696
697
698
699
700
701
702
703
704
705
706
707
708
709
710
711
712
713
714
715
716
717
718
719
720
721
722
723
724
725
726
727
728
729
730





731

732 **Fig. 4:** Depth slices through the new 3D shear-wave velocity model of the North Sea and surrounding
 733 landmasses at depths of 4, 8, 11, 15, 20 and 25 km. Labeled velocity anomalies '1-6'
 734 Dashed black line on (a) marks 4 km sediment thickness contour from EuCRUST-07 (Tesauro et al., 2008). A-
 735 A' and B-B' are the location of cross-section slices shown in Figure 6. See Supplementary Fig. 7 for slices at 30,
 736 35 and 40 km depth.

737

738

739

740

741

742

743

744

745

746

747

748

749

750

751

752

753

754

755

756

757

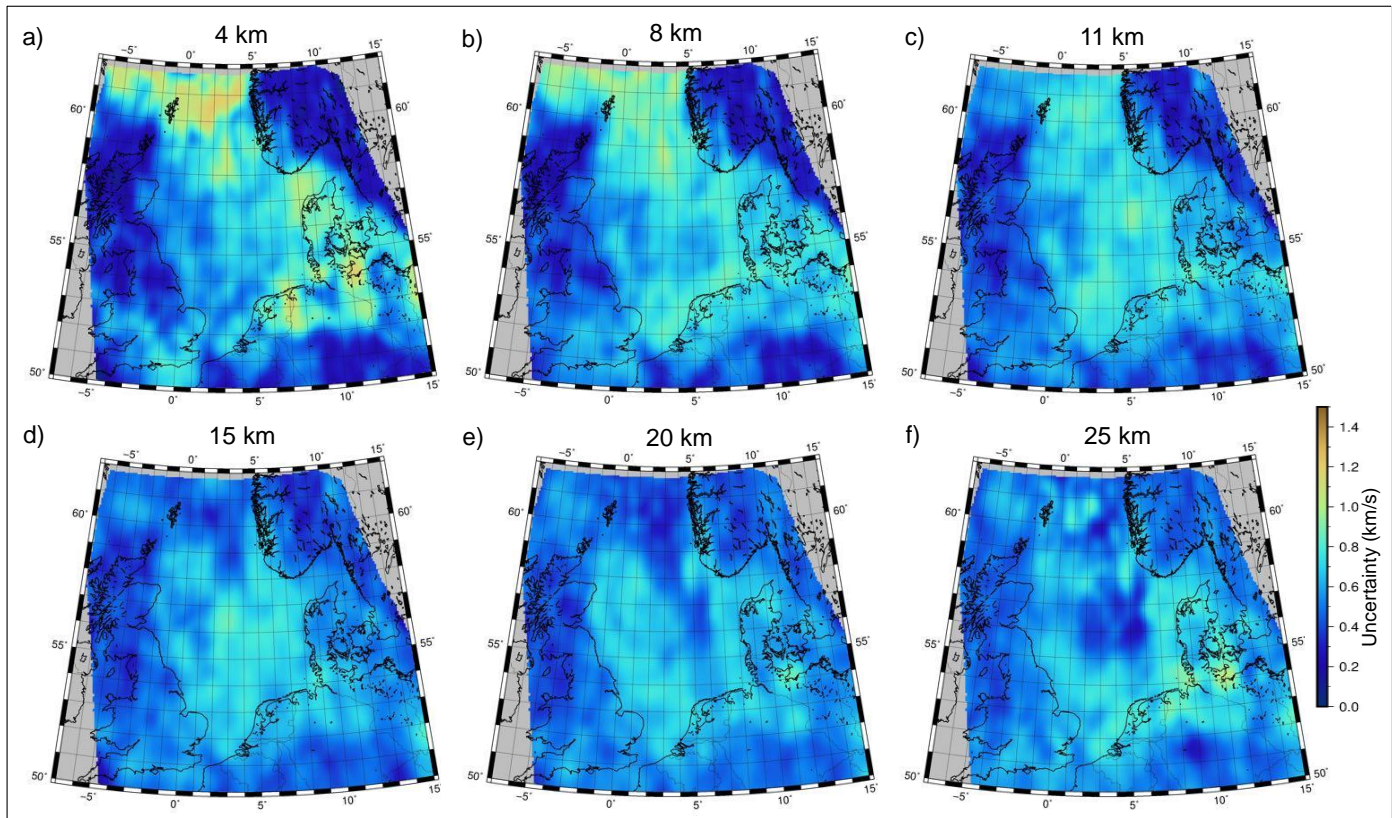
758

759

760

761

762



763

764

765

766 **Fig. 5:** Associated standard deviation values for the mean velocity model shown in Figure 4. Additional slices at

767 30, 35 and 40 km depth are shown in Supplementary Fig. 7.

768

769

770

771

772

773

774

775

776

777

778

779

780

781

782

783

784

785

786

787

788

789

790

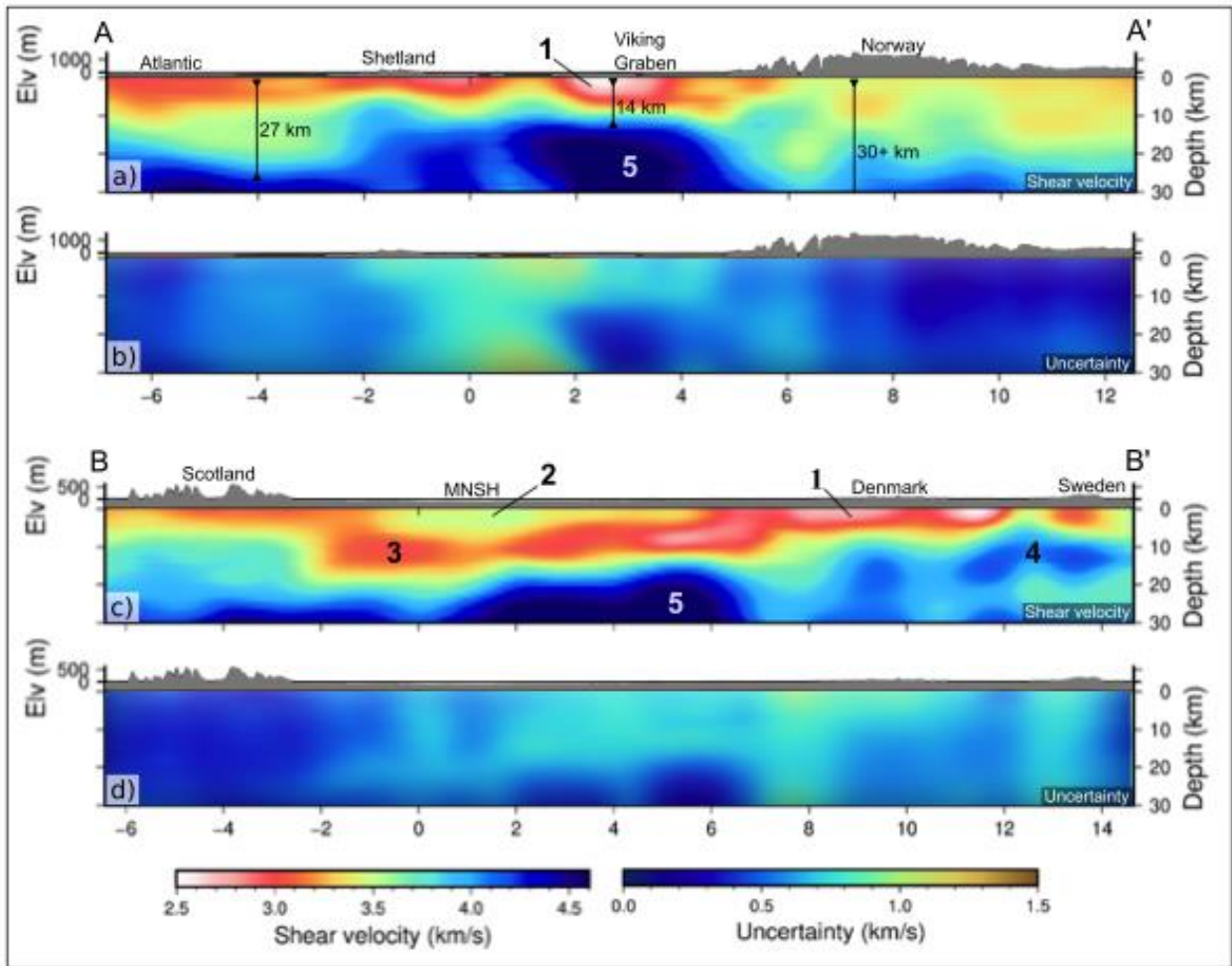
791

792

793

794

795



796

797

798

799**Fig. 6:** Cross-section slices through the new 3D shear-wave velocity model of the North Sea and surrounding
 800landmasses at latitudes of 56.0° and 60.0°. Labelled velocity anomalies '1-5' are discussed in the text.
 801Associated standard deviation values for the velocity model are shown below each cross-section. MNSH: Mid
 802North Sea High.

803

804

805

806

807

808

809

810

811

812

813

814

815

816

817

818

819

820

821

822

823

824
 825
 826
 827
 828
 829
 830
 831
 832
 833
 834
 835
 836
 837
 838
 839
 840
 841
 842
 843
 844
 845
 846
 847
 848
 849
 850
 851
 852
 853

